PROCEEDINGS OF SPIE

SPIEDigitalLibrary.org/conference-proceedings-of-spie

Terahertz planar surface plasmon interferometry

V. Gerasimov, V. Vanda, A. Lemzyakov, A. Ivanov, I. Azarov, et al.

V. Gerasimov, V. Vanda, A. G. Lemzyakov, A. I. Ivanov, I. A. Azarov, A. K. Nikitin, "Terahertz planar surface plasmon interferometry," Proc. SPIE 12776, Infrared, Millimeter-Wave, and Terahertz Technologies X, 127760C (26 November 2023); doi: 10.1117/12.2687247

SPIE.

Event: SPIE/COS Photonics Asia, 2023, Beijing, China

Terahertz planar surface plasmon interferometry

V. Gerasimov*[a,b], V. Vanda[a,b], A. G. Lemzyakov[a], A. I. Ivanov[c], I. A. Azarov[c] and A. K. Nikitin[d]
[a]Budker Institute of Nuclear Physics SB RAS, 11 Lavrentieva Ave., Novosibirsk, Russia 630090
[b]Dept. of Physics, Novosibirsk state university, 1, Pirogova Ave., Novosibirsk, Russia 630090
[c]Rzhanov Institute of Semiconductor Physics SB RAS, 13 Lavrentiev Aven., Novosibirsk, Russia 630090
[d]Scientific and Technological Centre of Unique Instrumentation RAS, 15 Butlerova Ave., Moscow, Russia 117342

ABSTRACT

Surface plasmon interferometry has found wide application in optical sensor devices in the visible range. In the THz region, where the surface plasmon polaritons (SPPs) propagation length extends to tens of centimeters, surface plasmon interferometers can be effectively used to control quality of the metal surface, to determine the effective permittivity of thin metal and dielectric coatings used in THz plasmonic integrated circuits, and for various sensor applications. The first THz SPP interferometer design and experimental results obtained with them in 130 to 358μm wavelength region for testing of metal surfaces and thin dielectric coatings deposited on it will be presented in this paper. The SPPs were generated by the Novosibirsk free electron laser coherent radiation on flat surfaces with gold sputtering, coated with ZnS layers of thickness from 0 to 3μm. Based on the measurement results, the value of the effective permittivity of the deposited gold was found; it turned out to be an order of magnitude smaller than that of bulk crystalline gold, which show the practical relevance of this method.

Keywords: terahertz spectral range, surface plasmon polaritons, surface plasmon interferometry, Michelson interferometer, refractometry, metal surfaces, plasmonic integrated circuits, coatings.

1. INTRODUCTION

Interferometry in beams of surface plasmon polaritons (SPPs), the kind of surface electromagnetic waves generated by a probing radiation on the surface of metals [1], enables combining the possibilities of amplitude and phase measurements for determination of the complex refractive index of SPPs, which is unambiguously related to the dielectric permittivity of the metal and optical constants of the transition layer [1, 2]. In addition, plasmonic interferometry enables study of fast processes on a conducting surface and can be efficiently used for sensor applications and in plasmonic microscopy [3, 4]. In the THz range plasmonic interferometers containing a metal (not a semiconductor) surface and thus using SPPs with large propagation length can be effectively applied for quality control of the surface of metal and metallized mirrors of macroscopic dimensions; determination of the effective permittivity of metal coatings used in THz plasmon waveguides, metasurfaces, and diffraction gratings; spectroscopy of thin dielectric films on a conducting surface; various sensor applications [5].
With the development of the technique of reflection and splitting of THz SPPs by flat mirrors and beam-splitting plates [6, 7], a scheme of a THz Michelson interferometer based on SPPs [8] was proposed, which was soon tested on FEL radiation [9]. The present work describes the design of the first terahertz Michelson interferometer based on SPPs, as are the results of identification of the effective permittivity of the deposited gold within its skin layer from the measured characteristics of the SPPs at a wavelength of 141 μm.

2. EXPERIMENTAL SETUP AND TEST RESULTS

2.1 Design of THz Michelson interferometer based on SPPs

Functioning of a THz SPP interferometer, like that of the classical Michelson interferometer, relies on analysis of interferogram. However, this interferogram is formed not by bulk waves, but by collinear SPP beams directed by the surface under study [8]. The real part n_s of the SPP refractive index is determined via comparison of the FEL emission

Infrared, Millimeter-Wave, and Terahertz Technologies X, edited by Cunlin Zhang, Yiwen E., Masahiko Tani, Proc. of SPIE Vol. 12776, 127760C · © 2023 SPIE
0277-786X · doi: 10.1117/12.2687247

spectrum with the SPP spectrum, resulting from the Fourier analysis of the interferograms. The imaginary part κ_s is governed by the attenuation of the intensity of SPPs as they propagate along the surface under study.

The source of THz radiation was the Novosibirsk Free Electron Laser (NovoFEL) [10], whose power (along with that of gyrotrons) is currently one of the highest. The NovoFEL radiation is a periodic sequence of 100-ps pulses following at a frequency of 5.6 MHz; it is linearly polarized and completely coherent in the beam cross section; the temporal coherence is 30−100 ps (depending on the operating mode of the laser). The characteristic average power of the radiation arriving at the interferometer input is 30−40 W (if necessary, it can be increased to 400 W); the Gaussian beam diameter is 12 mm. The operating radiation wavelength λ_0 was chosen to be 141 μm with a line width of less than 1%.

Because the spectrum of NovoFEL radiation is unstable in the normal mode of operation (the wavelength can shift by up to 0.2 μm during measurements), for the spectrum variations to be taken into account, the plasmonic interferogram was recorded simultaneously with the interferogram formed by the NovoFEL radiation beams. To this end, the Michelson interferometer for bulk waves was added to the scheme of the plasmonic interferometer [11] (Fig. 1a).

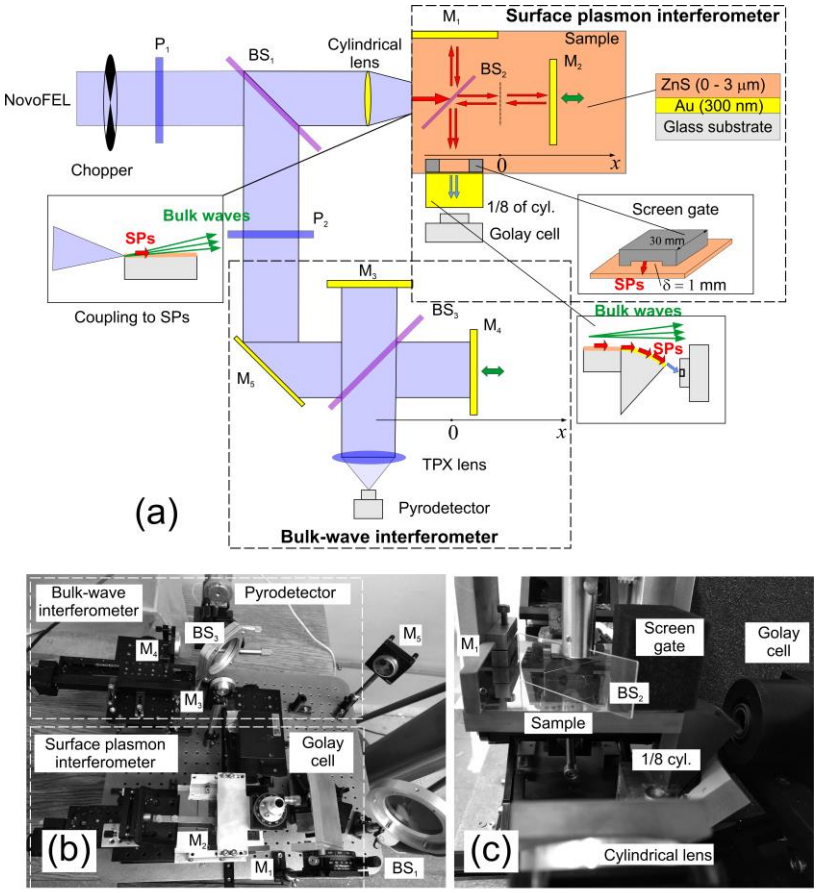

Figure 1. (a) Optical circuit (top view) of plasmonic THz interferometer: P1 and P2 – polarizers; BS1−BS3 − beam splitter; M1−M5 − flat mirrors; CL – cylindrical reflective lens; TPX lens – lens made of TPX; (b, c) top and side views of plasmonic interferometer.

The lithographic polarizer P1 extracted the *p* component, corresponding to the polarization of SPPs from the NovoFEL beam coming to the input of the setup. The 30-μm polypropylene film splitter BS1 separated the linearly polarized radiation into two beams. The mirror M5 directed the reflected beam, the intensity of which was controlled by the polarizer P2, to the bulk wave interferometer. The cylindrical metal reflecting lens CL with focal length of 75 mm focused the transmitted beam onto the upper edge of the end face of the flat substrate of the sample, where, due to diffraction, the radiation was converted into SPPs. In comparison with other known methods (generation on a diffraction grating, waveguide, or flat screen edge), the method of SPP generation on the edge of a flat substrate ("the end-fire

coupling technique" [12]) features high efficiency (tens of percent at sufficient overlapping of the incident wave fields and SPPs [13]), simplicity, and small dispersion of the conversion coefficient.

In the plasmonic interferometer, the fixed and movable mirrors M1 and M2 were used (40 × 20 × 5 mm glass plates with gold coating on the reflecting faces and ZnS protective layer). The splitter was the 40 × 25 × 1 mm plane-parallel plate BS2, made of polyimide material Zeonex (TYDEX, Russia) [14] and installed at an angle of 45° to the incident SPP beam. The lower faces of the mirrors and splitter were optically polished and adhered tightly to the substrate, providing optical contact with its surface. Unlike other well-known elements used to reflect or split SPPs (Bragg gratings [15] or geodesic prisms [16] formed on the sample surface), flat mirrors and splitters create much fewer parasitic bulk waves in interaction with SPPs [7]. In addition, such elements can be rearranged easily during reconfiguration of the interferometer.

As substrates for the test samples, 100×150×11 mm flat glass plates were used, the upper face of which (100–150 mm) was optically polished. An opaque layer of gold 300 nm thick was applied to it by magnetron sputtering, over which a layer of zinc sulfide (ZnS) of uniform thickness was deposited by electron beam evaporation. Three samples were fabricated: uncoated one and those with the ZnS layer of thickness d equal to 1.0 and 3.0 μm. Such a choice of samples was due to the significant difference (according to calculations) in the indices of refraction n_s and absorption κ_s of SPPs on these samples.

From the place of generation to the exit from the sample, the SPPs passed a distance of about 160 mm. At the output of the plasmonic interferometer, the combined SPP beams from both arms went to the convex surface of the cylindrical element (adjacent to the side face of the substrate) for conversion of the SPPs into bulk waves. The element was 1/8 of a cylinder with curvature radius of 60 mm, the convex surface of which contained a gold layer 300 nm thick coated by a ZnS layer 1.0 μm thick. The losses (mainly radiative) of the SPPs on the cylindrical surface were as high as 99%, although they were minimal at the chosen coating thickness [17]. Having reached the opposite edge of the convex face of the element, the SPPs diffracted on it and converted into bulk waves, which were recorded by the radiation detector. The interfering bulk waves generated by the SPPs beams on the free edge of the output coupling element were detected by the optoacoustic receiver (Golay cell GC-1T, TYDEX, Russia) with high sensitivity ($NEP \approx 1.4 \times 10{-}10$ W/Hz$^{1/2}$ [18, 19]) and sufficient operation speed (receiver response time of 30 ms).

In the interferometer for bulk waves, the beams lost energy insignificantly (only upon reflection from the splitter BS3). Therefore, interferograms of bulk waves were recorded by a less sensitive ($NEP \approx 1.9 \times 10{-}9$ W/Hz$^{1/2}$) single-pixel pyroelectric receiver MG-33 (NZPP Vostok, Russia) [20, 21], having however high speed (the typical time of receiver heating is about 10 μs [22] and the response time is about 5 ms). The radiation directed to its sensitive element of 1 × 1 mm in size was collected by the TPX lens (TYDEX, Russia) with focal length of 50 mm.

The movable mirrors M2 and M4 were attached to the platforms of motorized shifters (8MT175-50, Standa, Lithuania), which ensured motion of the mirrors during scanning along the x axis with a step of 2.5 μm. The scanning speed was chosen as the maximum possible (250 μm/s) at which the detectors had time to record signals correctly. The recording time for one pair of interferograms corresponding to a displacement of the movable mirrors by 15 mm was about 1 min.

Before experiments the SPP interferometer was aligned with collimated diode laser beam (λ = 635 nm) and THz beam of NovoFEL. Details of the alignment procedure are described detail in paper [11].

Figure 2a presents an example of plasmonic interferograms and interferograms of bulk waves recorded on the sample with d = 1.0 μm. As the movable mirrors of the interferometers are displaced along the x axis, the amplitudes of the sinusoids first increase, then reach the maximum, and decrease in the final section of the scanning. This is a typical symmetrical form of autocorrelation function for a coherent radiation source [23]. The amplitude envelope has a Gaussian profile, the width of which determines the length (time) of coherence, which was 30 mm (100 ps) in this experiment. This value coincides with the maximum duration of the NovoFEL radiation pulse during operation in a stable mode. Then the spectra of the SPs and NovoFEL radiation were calculated from the interferograms with application of the Fourier transform (Figure 2b). The empty dots in this figure indicate the results of calculations of the components of the Fourier spectrum. Note that the number of calculated points is governed by the interferogram length, which depends on the length of coherence of the NovoFEL radiation ($l_{coh} \approx 30$ mm). Next, the spectra were approximated with the Gaussian function of the form $f(x) = A \cdot \exp\left[-\frac{1}{2}\left(\frac{x - x_c}{w}\right)^2\right] + f_0$ and normalized to the value (A +

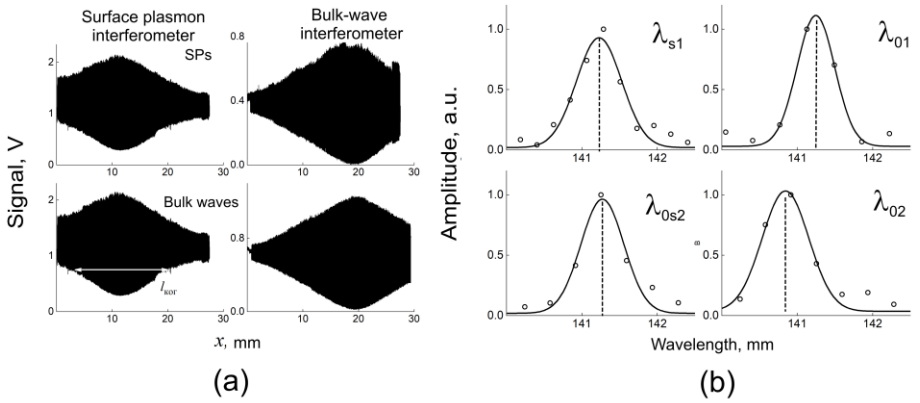

Figure 2. (a) Example of interferograms obtained with plasmonic interferometer (left) and bulk-wave interferometer (right) for sample "Au + ZnS layer 1.0 μm thick"; top row: graphs with SPP excitation; bottom row: graphs without SPP excitation; (b) Fourier spectra of SPPs and NovoFEL radiation generating them, reconstructed from interferograms in Fig. 2a (empty dots) and approximation of spectra by Gaussian function (solid curve).

f_0). The w value defines the spectrum width. The value of the parameter x_c, which determines the position of the central line of the spectrum, corresponds to the desired wavelength. The x_c value coincides completely with the results of the direct (but much more laborious) method of calculation of the wavelength from the average period of interferogram. The following wavelengths (central lines of the spectra) are marked in Figure 2b: λ_{s1} and λ_{0s2}, found from the interferograms in Figure 2a, obtained on the plasmonic interferometer with and without SPp excitation, respectively; λ_{01} and λ_{02} – corresponding to these interferograms wavelengths of NovoFEL radiation in air, determined with the use of the bulk-wave interferometer.

Since the complex refractive index of SPPs is defined as the ratio of the wave number k_s of SPPs to the wave number of the source radiation in vacuum $k_0 = 2\pi/\lambda_0$,

$$\tilde{n}_s = \frac{k_s}{k_0} = n_s + i \cdot \kappa_s, \tag{1}$$

the real part n_s can be found from the spectra presented in Figure 2b according to the following formula:

$$n_s = \left(\frac{\lambda_{п1}/\lambda_{0п2}}{\lambda_{o1}/\lambda_{o2}} \right) \cdot \mathrm{Re}\left(\tilde{n}_a\right), \tag{2}$$

where the ratio $\lambda_{s1}/\lambda_{0п}$ is defined by expression (1), and the normalization to $\lambda_{01}/\lambda_{02}$ takes into account the shift in the NovoFEL radiation spectrum that can occur during the time between recordings of interferograms with and without SPP excitation. The factor $\mathrm{Re}\left(\tilde{n}_a\right)$ in expression (2) makes it possible to take into account the fact that laser radiation propagates not in vacuum, but in air with the complex refractive index $\tilde{n}_a = 1.0002726 + i \cdot 0.0000039$ [24, 25]. For each sample, the average value of n_s was found for four sets of interferograms.

To find the κ_s value, we measured the decrease in the SPP intensity at displacement of the movable mirror M2 (see Figure 1) in the plasmonic interferometer; in this case, the fixed mirror M1 was covered by the absorbing plate. The characteristic form of the dependence measured on the sample with the ZnS layer 1 μm thick is shown in Figure 3. The same figure shows the result of approximation of the measurement results by a function of the form $g(x) = B \cdot \exp(-2x/L) + g_0$. The exponent indicator takes into account the fact that the SPP path increased by $2x$ when the mirror M2 was displaced by x. The noise level g_0 was measured experimentally and served as an approximation parameter (for the plot shown in Figure 3, the noise level was almost zero). For each sample, the average length L_{av} of SPP propagation was found from the results of several successive measurements (four measurements in our case), and the κ_s value was calculated by the formula [1]

$$\kappa_s = \frac{\lambda_0}{4\pi \cdot L_{av}}. \tag{3}$$

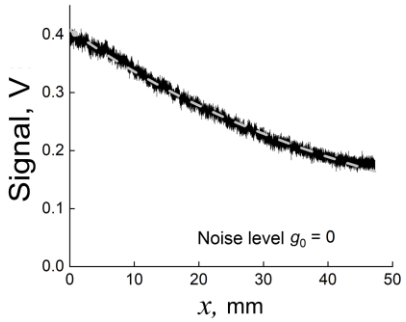

Figure 3. Attenuation of SP intensity on sample "Au + ZnS layer 1.0 μm thick" at displacement x of mirror M2 (see Fig. 1a) in plasmonic interferometer and fixed mirror M1 closed by absorber. Gray dashed line: result of exponential approximation.

2.2 Results of test measurements

Table 1 presents the values of the real (without unity) and imaginary parts of the refractive index of SPPs, found by formulas (2) and (3) for the three samples. For comparison, the same table shows the values of these quantities calculated from the SPP dispersion equation for the three-layer structure ("gold–ZnS layer–air") at λ_0 = 141 μm [11].

Table 1. Refractive indices of SPPs (real part without unity (n_s – 1) and imaginary part κ_s), calculated at substitution of experimental results into formulas (2) and (3), as well as their calculated values

Sample	n_s –1 (exp), $\times 10^{-4}$	n_s –1 (Drude), $\times 10^{-4}$	κ_s (exp.), $\times 10^{-4}$	κ_s (Drude), $\times 10^{-4}$
Au (d = 0)	4.9±4	2.7	1.5±0.1	0.014
Au+ZnS (d =1.0 μm)	14±2	10.5	1.1±0.1	0.400
Au+ZnS (d =3.0 μm)	98±10 (112±16 [26])	81.0	3.7±0.1 (6.6±0.7 [26])	1.300

According to Table 2, the experimental value of κ_s, which characterizes the losses of SPPs at propagation along the sample, is noticeably larger (especially at d = 0) than the respective calculated value. This can be because, in addition to the Joule losses in the metal, SPPs experience radiative losses on the roughness and optical inhomogeneities of the surface [27]. According to [27], the placement of a dielectric layer on the surface of conductor is expected to lead to decrease in the radiative losses of SPPs due to the larger difference between the refractive index n_s of SPPs and the refractive index of the source radiation in air. Moreover, at a sufficiently large thickness of the ZnS layer (d = 1.0 and 3.0 μm), the radiative losses become much lower than the Joule losses, which is expected to lead to coincidence of the calculated and experimental values of κ_s. However, according to Table 1, at d = 1.0 and 3.0 μm, the measured SPP losses are approximately three times higher than the calculated ones. It can also be seen that in the experiment the value of (n_s – 1) is consistently greater than the calculated values for the respective ZnS layer thicknesses. In our opinion, such discrepancies between the experiment and theory indicate that the effective permittivity of the metal surface differs from its values in crystalline metal calculated by the Drude model, which is most likely due to the granular structure of the surface of the deposited metal layer and its roughness. For the sample with d = 3.0 μm, the result for (n_s – 1) coincides within the error with the data of [26], which indicates the reliability of the measurements, whereas the calculated value of κ_s is two times less than the measured one, because the radiative losses of SPPs were not taken into account.

From the experimental values of (n_s – 1) and κ_s for a sample with a given thickness of the ZnS layer, one can determine the effective permittivity of the metal surface by solving dispersion equation numerically [28]. Table 2 presents solutions for the real and imaginary parts of the permittivity ε_m of the gold plating, found from the data in Table 1. The errors for ε_m correspond to the scatter of solutions to dispersion equation with the accuracy of determination of (n_s – 1) and κ_s taken into account. Table 2 also shows the gold permittivity values calculated by the Drude model with application of reference data for crystalline gold at λ_0 = 141 μm. As can be seen from the table, the experimental values of ε_m are less than the calculated ones by more than an order of magnitude. The largest difference (more than two orders of magnitude) is observed for uncoated gold (d = 0), which is due to the fact that the analytical model does not take into account the

radiative losses of SPPs, which are very substantial for SPPs on a conducting surface without a coating dielectric layer. More or less close values of ε_m are observed in the presence on the metal of the ZnS layer with thickness of 1.0 and 3.0 μm, when the radiative losses of SPPs are small. We made detail analysis of experimental results obtained with various ZnS dielectric thicknesses [28], which showed that for correct measurement of the optical constants of metal surface, it is necessary to use dielectric coatings of sufficient thickness. The large error for the found values of ε_m is mainly due to the insufficient temporal stability of the emission spectrum of NovoFEL [11].

Table 2. Values of real and imaginary parts of permittivity εm of sputtered gold, found from experimental values of (ns – 1) and κs from Table 1, as well as εm values calculated by Drude model at λ0 = 141 μm.

Sample	Re (ε_m) (exp)	Re (ε_m) (Drude)	Im (ε_m) (exp)	Im (ε_m) (Drude)
Au (d = 0)	-800±800	-105000	1700±1500	317000
Au+ZnS (d=1.0 μm)	-5600±3600		2600±1400	
Au+ZnS (d =3.0 μm)	-7000±5000		1000±800	

3. SUMMARY

The paper presents the optical circuit of a planar THz SPP Michelson interferometer. A technique for determination of the complex refractive index of SPPs ($\tilde{n}_s = n_s + i\kappa_s$) from interferograms is described. The interferometer was tested on flat surfaces with gold sputtering coated with a ZnS layer 0 to 3.0 μm thick with application of high-power coherent radiation of NovoFEL at the wavelength λ_0 = 141 μm. From the found values of the effective permittivity ε_m of the deposited gold surface was calculated, which turned out to be an order of magnitude lower than that of crystalline gold. The large error for the found values of ε_m is mainly due to the insufficient temporal stability of the emission spectrum of NovoFEL. For practical applications of the plasmonic interferometer, it is necessary to use more stable and compact sources of THz radiation.

ACKNOWLEDGMENTS

The work was done on the equipment of the shared research center SSTRC on the basis of the Novosibirsk FEL at BINP SB RAS. The authors acknowledge core facilities “VTAN” (Novosibirsk State University) for the access to its experimental equipment.

REFERENCES

[1] Agranovich, V.M. and Mills, D.L., Poverkhnostnye polyaritony. Elektromagnitnye volny na poverkhnostyakh i granitsakh razdela sred (Surface Polaritons. Electromagnetic Waves on Surfaces and Media Boundaries), Nauka, Moscow (1985).
[2] Maier, S.A., Plasmonics−Fundamentals and Applications, Springer, New York (2007).
[3] A. N. Nikitina and A. A. Tishchenko, Pis’ma Zh. Tekh. Fiz. 17 (11), 76 (1991).
[4] Zhu, J., Xie, X., Sun, M., Bi, Q., and Kang, J., “A Novel Femtosecond Laser System for Attosecond Pulse Generation,” Advances in Optical Technologies 2012, 1–6 (2012).
[5] Azarov, I.A., Shvets, V.A., Prokopiev, V.Yu., Dulin, S.A., Rykhlitskii, S.V., Choporova, Yu.Yu., Knyazev, B.A., Kruchinin, V.N., and Kruchinina, M.V., “A terahertz ellipsometer,” Instruments and Experimental Techniques 58(3), 381–388 (2015).
[6] Gerasimov, V.V., Knyazev, B.A., and Nikitin, A.K., “Reflection of terahertz monochromatic surface plasmon-polaritons by a plane mirror,” Quantum Electronics 47(1), 65–70 (2017).

[7] Gerasimov, V.V., Nikitin, A.K., Lemzyakov, A.G., Azarov, I.A., Milekhin, I.A., Knyazev, B.A., Bezus, E.A., Kadomina, E.A., and Doskolovich, L.L., "Splitting a terahertz surface plasmon polariton beam using Kapton film," Journal of the Optical Society of America B 37(5), 1461 (2020).
[8] Nikitin, A.K. and Khitrov, O.V., RF Patent 2709600, Byull. Izobret., 35 (2019).
[9] Gerasimov, V.V., Nikitin, A.K., Khitrov, O.V., and Lemzyakov, A.G., "Experimental Demonstration of Surface Plasmon Michelson Interferometer at the Novosibirsk Terahertz Free-Electron Laser," Proc. 6th Int. Conference on Infrared, Millimeter, and Terahertz Waves (IRMMW-THz), Chengdu, August 29–September 3, 1 (2021).
[10] Shevchenko, O.A., Vinokurov, N.A., Arbuzov, V.S., Chernov, K.N., Davidyuk, I.V., Deichuly, O.I., Dementyev, E.N., Dovzhenko, B.A., Getmanov, Ya.V., et al., "The Novosibirsk Free-Electron Laser Facility," Bulletin of the Russian Academy of Sciences: Physics 83(2), 228–231 (2019).
[11] Gerasimov, V.V., Nikitin, A.K., and Lemzyakov, A.G., "Planar Michelson Interferometer Using Terahertz Surface Plasmons," Instruments and Experimental Techniques 66(3), 423–434 (2023).
[12] Stegeman, G.I., Wallis, R.F., and Maradudin, A.A., "Excitation of surface polaritons by end-fire coupling," Optics Letters 8(7), 386 (1983).
[13] Gerasimov, V.V., Nikitin, A.K., Lemzyakov, A.G., and Azarov, I.A., "Evaluation of the Efficiency of Generation of Terahertz Surface Plasmon Polaritons by the End-Fire Coupling Technique," Photonics 10(8), 917 (2023).
[14] Islam, M.S., Cordeiro, C.M.B., Nine, M.J., Sultana, J., Cruz, A.L.S., Dinovitser, A., Ng, B.W.-H., Ebendorff-Heidepriem, H., Losic, D., et al., "Experimental Study on Glass and Polymers: Determining the Optimal Material for Potential Use in Terahertz Technology," IEEE Access 8, 97204–97214 (2020).
[15] Nazarov, M., Garet, F., Armand, D., Shkurinov, A., and Coutaz, J.-L., "Surface plasmon THz waves on gratings," Comptes Rendus Physique 9(2), 232–247 (2008).
[16] Knyazev, B.A. and Nikitin, A.K., RF Patent 2547164, Byull. Izobret., 10 (2015).
[17] Knyazev, B.A., Gerasimov, V.V., Nikitin, A.K., Azarov, I.A., and Choporova, Yu.Yu., "Propagation of terahertz surface plasmon polaritons around a convex metal–dielectric interface," Journal of the Optical Society of America B 36(6), 1684 (2019).
[18] Siberian State University of Geosystems and Technologies, Minin, I.V., Minin, O.V., and Siberian State University of Geosystems and Technologies, "Millimeter and terahertz radiation detector," Vestnik SSUGT (Siberian State University of Geosystems and Technologies) 26(4), 160–175 (2021).
[19] http://www.tydexoptics.com/ru/products/thz_devices/golay_cell/.
[20] http://www.nzpp.ru/product/gotovye-izdeli/fotopriemnye- ustroystva/.
[21] Paulish, A.G., Dorozhkin, K.V., Gusachenko, A.V., Morozov, A.O., and Pyrgaeva, S.M., Sbornik trudov konferentsii "Aktual'nye problemy radiofiziki APR 2019" (Proc. Conference "Topical Problems on Radio-Physics APR 2019"), Tomsk, 482 (2019). http://vital.
[22] Zubov, V.A., "Metody izmereniya kharakteristik lazernogo izlucheniya" (Methods for Measuring Characteristics of Laser Emission), Moscow: Nauka (1973).
[23] Kubarev, V.V., Kulipanov, G.N., Kolobanov, E.I., Matveenko, A.N., Medvedev, L.E., Ovchar, V.K., Salikova, T.V., Scheglov, M.A., Serednyakov, S.S., et al., "Modulation instability, three mode regimes and harmonic generation at the Novosibirsk terahertz free electron laser," Nuclear Instruments and Methods in Physics Research Section A: Accelerators, Spectrometers, Detectors and Associated Equipment 603(1–2), 25–27 (2009).
[24] Mathar, R.J., "Refractive index of humid air in the infrared: model fits," Journal of Optics A: Pure and Applied Optics 9(5), 470–476 (2007).
[25] Burke, J.J., Stegeman, G.I., and Tamir, T., "Surface-polariton-like waves guided by thin, lossy metal films," Physical Review B 33(8), 5186–5201 (1986).
[26] Gerasimov, V.V., Knyazev, B.A., Nikitin, A.K., Nikitin, V.V., and Rijova, T.A., "Interference Refractometry of Terahertz Surface Plasmon-Polaritons Launched by a Free-Electron Laser," Discrete and Continuous Models and Applied Computational Science, 2, 191-200 (2013). https://journals.rudn.ru/miph/article/view/8543.
[27] Gerasimov, V.V., Knyazev, B.A., Lemzyakov, A.G., Nikitin, A.K., and Zhizhin, G.N., "Growth of terahertz surface plasmon propagation length due to thin-layer dielectric coating," Journal of the Optical Society of America B 33(11), 2196 (2016).
[28] Gerasimov, V.V., Nikitin, A.K., Lemzyakov, A.G., Azarov, I.A., and Kotelnikov, I.A., "Obtaining the Effective Dielectric Permittivity of a Conducting Surface in the Terahertz Range via the Characteristics of Surface Plasmon Polaritons," Applied Sciences 13(13), 7898 (2023).